Acta Geochim
https://doi.org/10.1007/s11631-024-00684-4

ORIGINAL ARTICLE

Zircon U–Pb geochronologic, geochemical and Sr–Nd–Pb isotope characteristics of the Beidaban granites in the North Qilian Orogenic Belt: Petrogenesis and tectonic implications

Tao Yang[1] · Zhi-yuan Sun[2] · Ming-liang Wang[2] · Xiao-qiang Zhu[3] · Jing-yu Zhao[2]

Received: 16 November 2023 / Revised: 21 February 2024 / Accepted: 10 March 2024

Abstract The tectonic evolution and crustal accretion process of the North Qilian Orogenic Belt (NQOB) are still under debate because of a lack of integrated constraints, especially the identification of the tectonic transition from arc to initial collision. Here we present results from zircon U–Pb geochronology, whole-rock geochemistry, and Sr–Nd–Pb isotope geochemistry of the Beidaban granites to provide crucial information for geodynamic evolution of NQOB. Zircon U–Pb dating yields an age of 468 ± 10 Ma for the Beidaban granites and most of the Beidaban samples contain amphibole, are potassium-rich, and have A/CNK values ranging from 0.7 to 0.9, illustrating that the Middle Ordovician Beidaban granites are K-rich, metaluminous, calc-alkaline granitoid. The geochemical characteristics indicate that the Beidaban granites are transitional I/S-type granitoids that formed in an arc setting. The isotopic compositions of initial $(^{87}Sr/^{86}Sr)_i$ values ranging from 0.70545 to 0.71082 (0.70842 on average) and εNd(t) values ranging from −10.9 to −6.7 (−8.8 on average) with two-stage Nd model ages (T_{DM2}) of 1.74–2.08 Ga suggest that the Beidaban granites originated from Paleoproterozoic crustal materials. In addition, the initial Pb isotopic compositions ($^{206}Pb/^{204}Pb = 19.14–20.26$; $^{207}Pb/^{204}Pb = 15.71–15.77$; $^{208}Pb/^{204}Pb = 37.70–38.26$) and geochemical features, such as high Th/Ta (17.43–30.12) and Rb/Nb (6.01–15.49) values, suggest that the Beidaban granite magma source involved recycled crustal components with igneous rocks. Based on these results in combination with previously published geochronological and geochemical data from other early Paleozoic igneous rocks, we suggest that the timing of the tectonic transition from arc to the initial collision to the final closure of the North Qilian Ocean can be constrained to the Middle-Late Ordovician (ca. 468–450 Ma).

Keywords Granitoids · Zircon U–Pb dating · Sr–Nd–Pb-isotopes · Petrogenesis · North Qilian Orogenic Belt

1 Introduction

The Qilian Orogenic Belt (QOB), located along the northeastern margin of the Tibetan Plateau, is a suture zone that has recorded an evolutionary history from continental breakup, oceanic subduction, and continental collision from the Proterozoic to the Paleozoic (Yin and Harrison 2000; Song et al. 2013; Liu et al. 2018; Wang et al. 2020). The North Qilian Orogenic Belt (NQOB) is a typical Early Paleozoic orogenic belt in the QOB, and studies have demonstrated that long-lived magmatism occurred during multiple episodes of orogenic processes in the Paleozoic (Xiao et al. 2009; Song et al. 2013, 2014; Zuza et al. 2017). The Paleozoic ophiolite sequences, island arc and collision-related granitoids, high-pressure metamorphic rocks, Silurian flysch formations, and Devonian molasses record the evolution from the subduction and closure of the North Qilian Ocean to the collision between the Qilian-Qaidam block and Alxa block (Song et al. 2013). Although intensive scientific research (Song et al. 2006, 2013; Wu et al. 2010; Yu et al. 2015; Yuan and Yang 2015; Zeng et al. 2016; Zhang et al. 2017; Wang et al. 2019) regarding the geodynamic events

✉ Zhi-yuan Sun
sunzhiyuan010@163.com

[1] The First Institute of Geology and Mineral Exploration, Gansu Provincial Bureau of Geology and Mineral Exploration, Tianshui 741020, China

[2] School of Resources and Civil Engineering, Suzhou University, Suzhou 234000, China

[3] School of Geography and Tourism, Anhui Normal University, Wuhu 241000, China

Published online: 05 April 2024

of the NQOB has focused on interpreting Paleozoic orogenic processes, several important issues, such as subduction polarity, timing of transition from subduction to collision, and closure of the North Qilian Ocean, are still debated.

As an important part of the continental crust, granites have been intensively studied because they contain valuable information about crustal evolution, crust–mantle interactions, and mountain building (Lundstrom and Glazner 2016; Wu et al. 2007; Hopkinson et al. 2017; Wang et al. 2018). The petrogenesis, source, evolution, and tectonic setting of granites have long been important topics in research on the evolutionary history and tectonic attributes of orogenic belts (Chappell and White 1974; Pearce et al. 1984; Clemens 2003; Zhu et al. 2009; Xu et al. 2010; Chen et al. 2018; Li et al. 2022). Lithologically, Early Paleozoic granites are widespread in the NQOB and are of utmost importance in understanding the tectonic evolution (Tseng et al. 2009; Yu et al. 2015). In addition, the identification of different types of granites can be used to reconstruct key geodynamic processes, such as the initial timing of the transition from arc to collision during subduction (Wang et al. 2018; Zhao et al. 2022) and the transition from compression to extension during collision (Yu et al. 2015; Zeng et al. 2016; Zhang et al. 2017). In this contribution, we conducted integrated research on the zircon geochronology and whole-rock geochemistry of the Early Paleozoic Beidaban granites in the NQOB. Based on this work, combined with previously published geochronological and geochemical data on Early Paleozoic igneous rocks (ca. 468–414 Ma), the purpose of this study is to better constrain their sources and petrogenesis, to improve our understanding of their tectonic evolution history, and to provide new constraints on the Early Paleozoic transitional tectonic events of the NQOB.

2 Geological background

The QOB is located at the intersection of the Alxa block, Tarim block, North China block, and Qaidam block (Fig. 1). It has experienced multiple episodes of tectonic evolution, including continental breakup, ocean basin formation, oceanic subduction, arc, back-arc systems, and continental collision (Xiao et al. 2009; Zuza et al. 2017; Zhu et al. 2022). The QOB consists of three nearly parallel tectonic subunits trending NW–SE from south to north: the South Qilian Orogenic Belt (SQOB), the Central Qilian Block, and the NQOB (Fig. 1) (Xia et al. 2016; Li et al. 2018; Gao et al. 2021). The SQOB is bounded by the Zongwulong Orogenic Belt, the Quanji Massif, and the North Qaidam ultrahigh-pressure metamorphic belt of

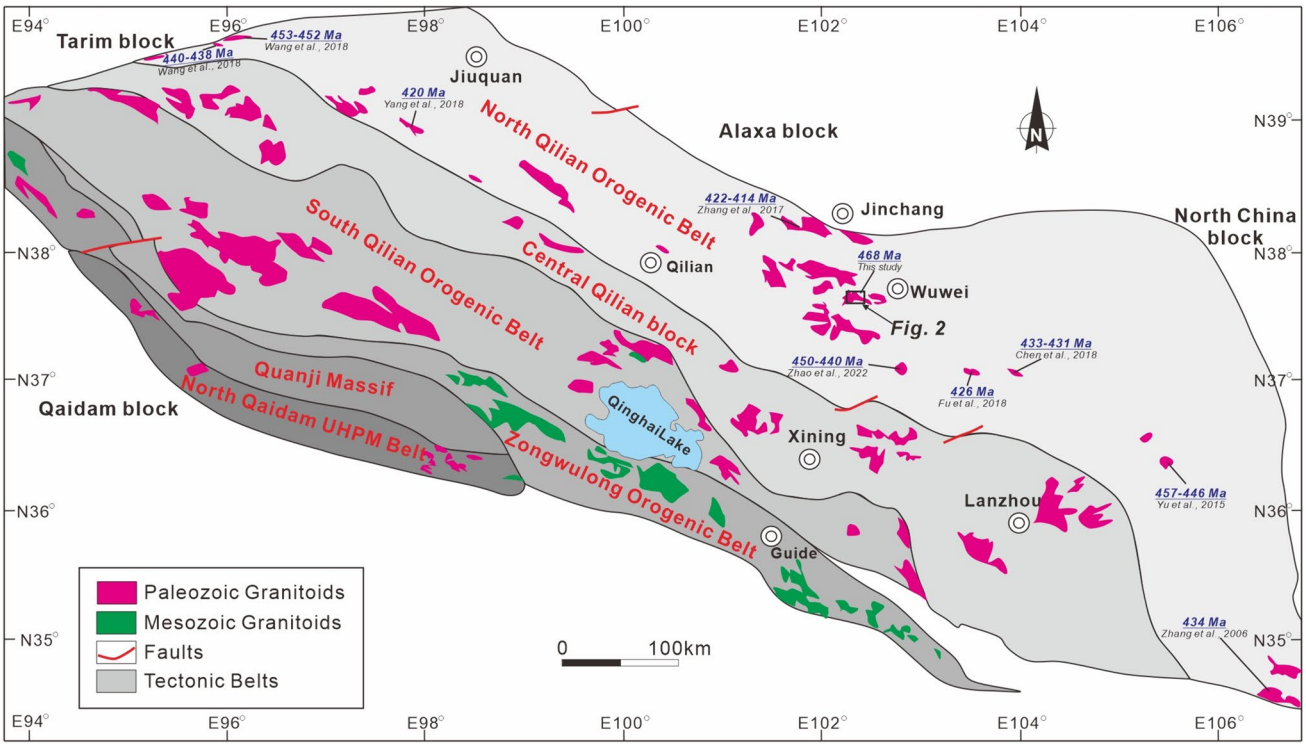

Fig. 1 Schematic map showing major tectonic units of the Qilian Orogenic Belt. The simplified geological map of the Qilian Orogenic Belt was modified from Zhu et al. (2022) by showing main boundaries of tectonic units and distribution of Paleozoic and Mesozoic granitoids rather than other tectonic units such as volcanics, sedimentary strata, and mafic–ultramafic rocks

the Qaidam Block. This belt was thought to constitute the final suture zone in the Qilian-Qaidam region (Song et al. 2009; Yang et al. 2018). The Central Qilian Block mainly consists of Precambrian high-grade granitic gneisses and low-grade metamorphic assemblages, overlain by Paleozoic sedimentary rocks and intruded by granitoids (Smith 2006; Huang et al. 2015; Fu et al. 2018).

The NQOB is situated in the northern part of the QOB and bounded by the Alxa block to the north (Fig. 1). The NQOB consists of two Early Paleozoic ophiolite belts (southern ophiolite belt (550–497 Ma, representing the spreading of the Oceanic basin) and a northern ophiolite belt (490–448 Ma, representing the back-arc basin extension), arc-related volcanic and intrusive rocks, high pressure metamorphic rocks, and accretionary complexes (Pan et al. 2004; Smith and Yang 2006; Song et al. 2007, 2013; Zhang et al. 2007; Xiao et al. 2009; Lin et al. 2010; Xia et al. 2012; Cheng et al. 2016; Li et al. 2017), which represent a typical western Pacific-type trench-arc-basin system. This zone is regarded as a suture zone resulting from the subduction of the North Qilian Ocean between the Alxa terrane and the Central Qilian Block in the Early Paleozoic (Xia et al. 2003, 2012; Song et al. 2007, 2013; Zhang et al. 2007; Li et al. 2016; Peng et al. 2017; Zhu et al. 2022).

Early Paleozoic intrusions are widespread throughout the NQOB. The Beidaban granite mass in the study area is located in the central part of the NQOB (Fig. 1). Cambrian metamorphic basement rocks, Early Paleozoic intrusive rocks, and Paleozoic to Mesozoic sedimentary sequences developed in the study area (Fig. 2). The oldest Cambrian Dahuangshan Group consists of metamorphosed feldspathic quartz sandstone and meta-arkose interbedded with low-grade metamorphosed slate. Ordovician and Silurian strata are absent in the study area. Carboniferous sedimentary rocks consist of clastic deposits of shallow marine and marine terrigenous facies with carbon-rich shale, sandstone, and coal. The conformable overlying these sedimentary rocks are Permian strata, which are mainly distributed in the southwestern part of the study area. The Permian rocks probably represent coarse clastic sediments (quartz sandstone and feldspathic sandstone) deposited in braided rivers. Jurassic strata consist of clastic rocks interbedded with sandstone and coal layers. The faults in the study area trend toward the SN and EW. Intermediate-acidic intrusive rocks are widely exposed on the northern side of the study area and include diorite, granodiorite, granite, monzogranite, and syenogranite (Chen et al. 2019). The Beidaban granite, with an exposed area of approximately 285 km^2, is located in Jinshan town, Wuwei City, Gansu Province (Fig. 2).

3 Occurrence and petrography of granite samples

The Beidaban granite samples collected in the field are penetratively deformed by the development of spaced cleavage (Fig. 3a). The granite samples are pale red or pink in color and feature fine- to medium-grained granitic textures. They are mainly composed of euhedral K-feldspar (35%–40%), euhedral plagioclase (15%–20%), subhedral to anhedral quartz (25%–30%), and minor amphibole (3%–5%) and biotite (2%–3%) (Fig. 3b). Accessory minerals include small amounts of Ti–Fe oxides, allanite, apatite, and zircon.

The K-feldspars are characterized by large euhedral laths or subhedral crystals that are 500–2000 μm in diameter (Fig. 3c, d). Most of them are microcline with typical tartan twinning. The plagioclase grains commonly exhibit euhedral to subhedral shapes and polysynthetic twinning and Carlsbad twinning, and they are generally 200–2000 μm in diameter (Figs. 3c, d). The plagioclase grains with hydromicazation on the surface are likely andesines (An = 32–40) based on the maximum extinction angle of the plagioclase crystals. Myrmekitic intergrowth of oligoclase and wormy quartz is common (Fig. 3c). The monocrystalline quartz crystals are typically subhedral to euhedral crystals ranging from 200 to 1000 μm in diameter (Fig. 3e). Amphiboles exist as perfect euhedral crystals in the Beidaban granite (Fig. 3e, f). They are mainly hexagonal and rhomboid in shape, and some are replaced by chlorite and carbonate minerals. The biotites are predominantly associated with amphiboles and display subhedral to euhedral crystals (Fig. 3e). Most of the biotites are replaced by chlorite. Minor Ti–Fe oxides with grain sizes ranging from 100 to 300 μm are occasionally observed in the Beidaban granite (Fig. 3f).

4 Analytical methods

Zircon grains for the laser ablation inductively coupled plasma mass spectrometry (LA-ICP-MS) analyses were separated using conventional magnetic and density techniques and then selected under a binocular microscope. The hand-picked zircon grains from the granite samples were mounted in epoxy and then polished to expose cross sections. Zircons under reflected and transmitted light, and cathodoluminescence (CL) were imaged to examine the internal microstructures. Before the experiment, zircons with clear oscillatory zoning structures were selected. LA-ICP-MS zircon U–Pb dating was conducted at the Tianjin Institute of Geology and Mineral Resources, Chinese Geological Survey. The detailed analysis involved a 193 nm laser ablation system coupled with an Agilent 7500 ICP-MS. Helium was taken as the carrier to enhance the transport efficiency of the ablated materials. A 32 μm spot size was used with an energy density of 5 J/cm^2 and a

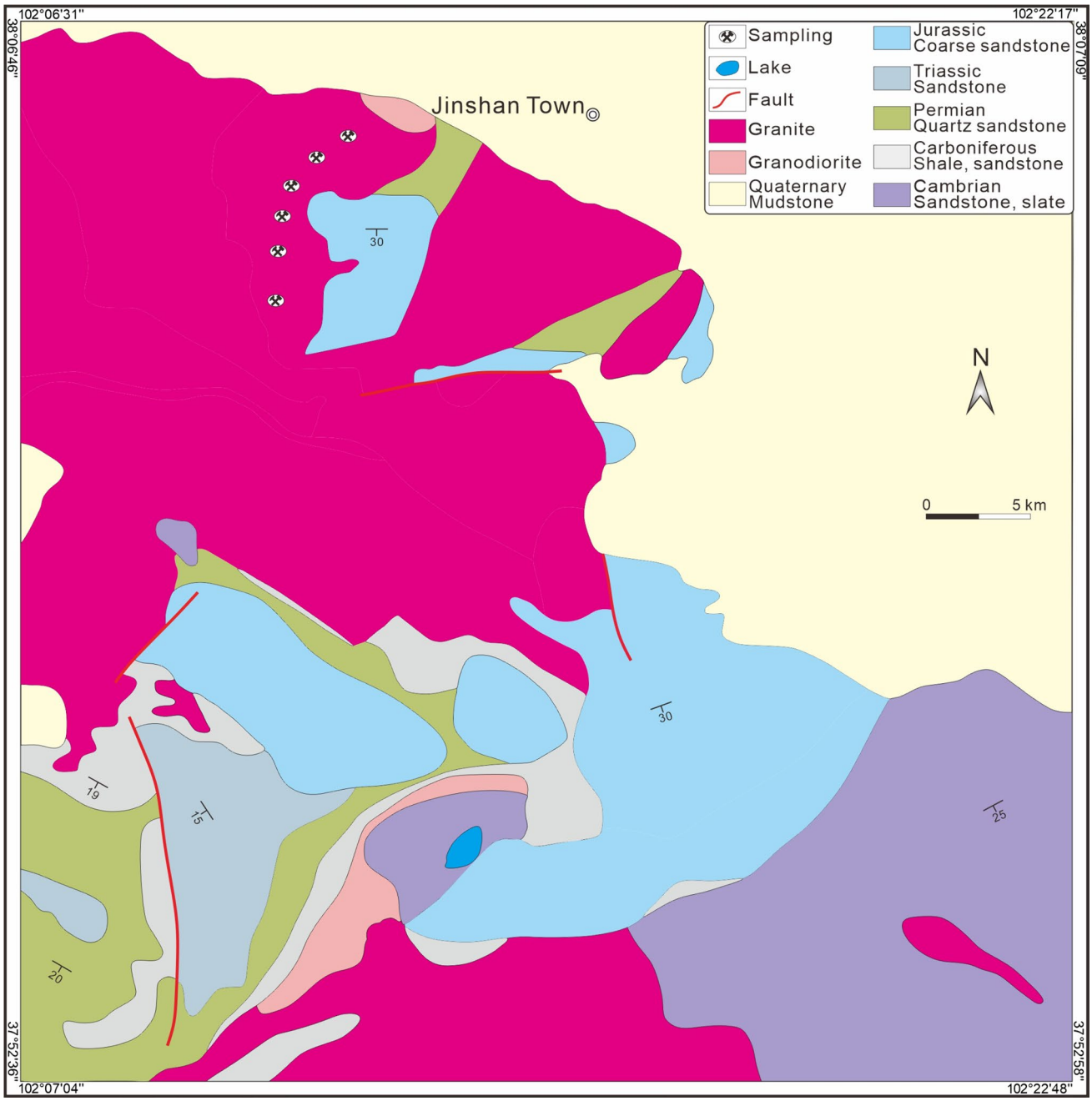

Fig. 2 Geological map of Beidaban pluton in the NQOB with localities of representative samples (modified from 1:50 000 geological map of Beidaban and surrounding areas)

repetition rate of 5 Hz. The U, Th, and Pb concentrations were calibrated using ^{29}Si as an internal standard, and NIST 610 as a reference standard. Zircon 91500 was used as the external standard for U–Pb dating. Time-dependent drifts of U-Th-Pb isotope ratios were corrected using linear interpolation for every ten analyses. Data reduction was performed using the ICPMSDataCal software (Liu et al. 2008). Only data with a concordance in the range of 90%–110% were considered for interpretation of zircon ages. Concordia diagrams were produced using ISOPLOT 3.0 software (Ludwig 2003).

The analyses of major and trace elements (including rare earth elements) of the granite samples were performed at the Tianjin Institute of Geology and Mineral Resources, Chinese Geological Survey. In the process of major element analysis, samples were first weighed into moderate amounts of boric acid and then melted into glass at high temperatures. Then, the oxide contents were measured via an XRF instrument

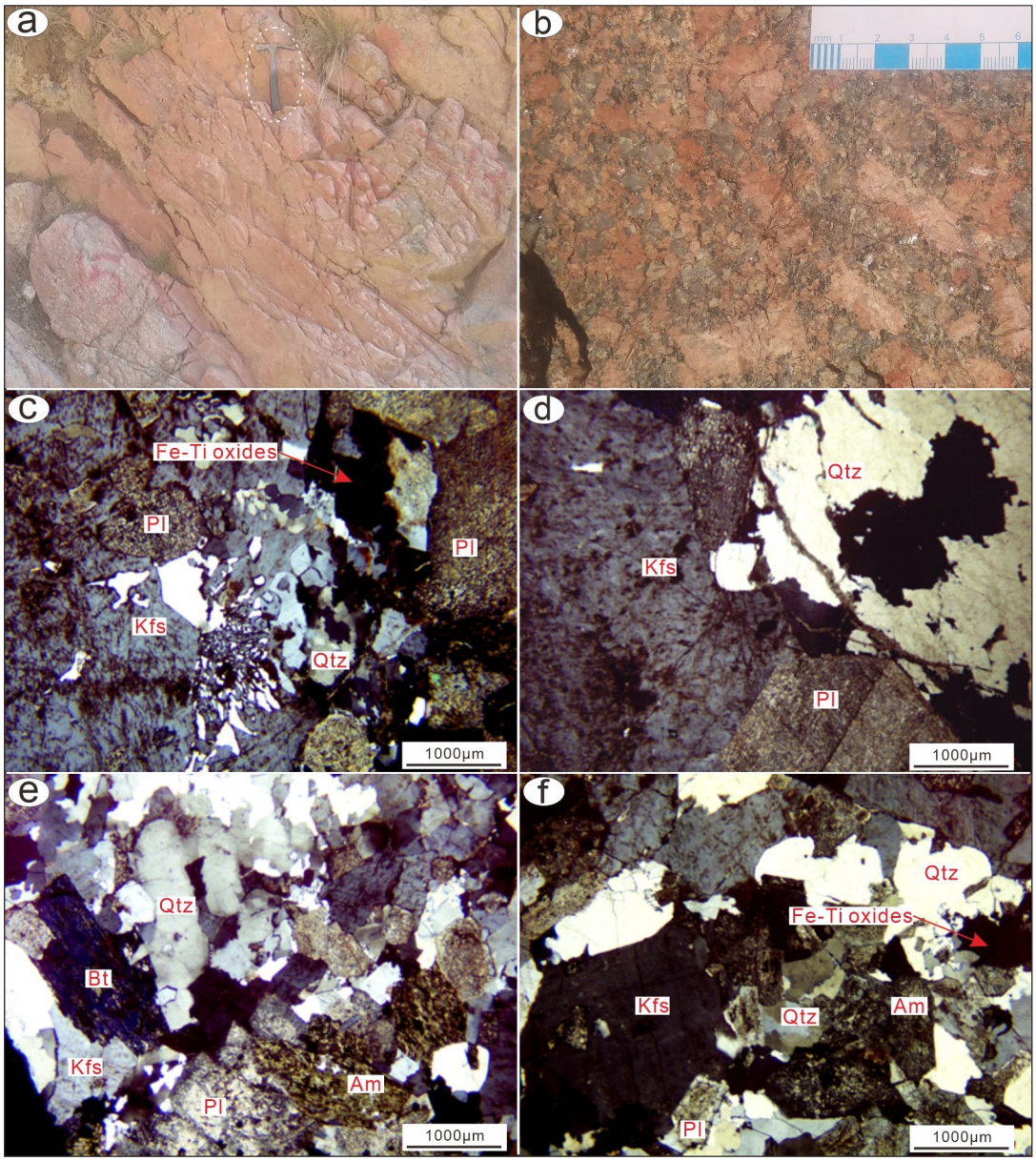

Fig. 3 Field (**a**–**b**) and thin-section (**c**–**f**) photographs of the Beidaban granites. **a** and **b** showing the establishing shot and close shot of granite; **c**–**f** showing the mineral assemblage of granite; Abbreviations: Pl–plagioclase; Kfs–K-feldspar; Qtz–quartz; Am–amphibole; Bt–biotite

and the analysis accuracy was better than 1%. The trace element analysis was completed via an inductively coupled plasma mass spectrometer (ICP-MS) with Finnigan MAT Element I equipment according to the procedure for DZ/T0223-2001 ICP-MS. The relative error of the analysis element was better than ± 5%, the temperature and humidity during the progression of the experiment were 20 °C and 30%, respectively.

Whole-rock Sr–Nd isotopic compositions were analyzed at the Tianjin Institute of Geology and Mineral Resources, Chinese Geological Survey, using a multi-collector VG 354 mass spectrometer in static mode. Approximately 100–150 mg of powder was decomposed in a mixture of HF–$HClO_4$ in screw-top Teflon beakers, and Rb, Sr, Sm, and Nd were separated using cation exchange columns. The Sr and Nd isotopic fractionations were corrected to $^{6}Sr/^{88}Sr = 0.1194$ and $^{146}Nd/^{144}Nd = 0.7219$, respectively. During the analytical period, several measurements of the NIST NBS987 Sr reference standard and the JNdi-1 Nd reference standard yielded $^{87}Sr/^{86}Sr = 0.710232 \pm 15$ (2σ) and $^{143}Nd/^{144}Nd = 0.512117 \pm 11$ (2σ), respectively. Analytical precision is approximately 1% for $^{87}Rb/^{86}Sr$ and 0.5% for $^{147}Sm/^{144}Nd$. Detailed sample preparation and

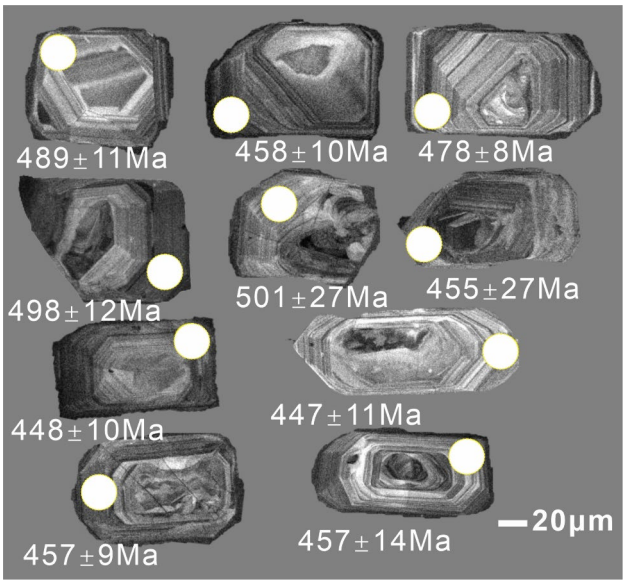

Fig. 4 Representative cathodoluminescence (CL) images of measured zircons from the Beidaban granites

analytical procedures for Sr and Nd isotopic analysis followed those of Tang et al. (2007) and He et al. (2007).

Whole-rock Pb was separated and purified using anion exchange in HCl–Br columns. The Pb isotopic ratios of granite samples were measured via MC-ICP-MS on a Nu Instruments system in the same laboratory as the Sr and Nd isotopic analysis. Pb isotopic fractionation was corrected to $^{205}Tl/^{203}Tl = 2.3875$. During the analytical period, repeated analyses of international standard NBS981 yielded ratios of $^{206}Pb/^{204}Pb = 16.939 \pm 0.013$ (2σ), $^{207}Pb/^{204}Pb = 15.497 \pm 0.011$ (2σ), and $^{208}Pb/^{204}Pb = 36.712 \pm 0.033$ (2σ), respectively. Detailed sample preparation and analytical procedures for the Pb isotope measurements followed those of He et al. (2005).

5 Results

5.1 Zircon U–Pb geochronology

Zircon grains from the Beidaban granite samples are euhedral and display similar crystal forms with long axes varying from 80 to 150 μm and length/width ratios ranging from 1 to 2 (Fig. 4). Cathodoluminescence (CL) images reveal that all zircon grains exhibit homogeneous oscillatory growth zoning, which is interpreted as typical magmatic features. Ten zircons from the granite samples were analyzed, and the individual zircon U–Pb dating results, U and Th contents, and isotopic ratios are listed in Table 1. The zircons have U contents ranging from 198 to 1180 ppm (632 ppm on average) and Th/U ratios ranging from 0.5 to 0.9, indicating

Table 1 Zircon U–Pb isotopic data from the Beidaban granites

Sample	Element (ppm)			Ratios	Isotopic ratios								Age (Ma)							
	U	Th	Pb	Th/U	$^{207}Pb/^{235}U$	2σ	$^{206}Pb/^{238}U$	2σ	$^{207}Pb/^{206}Pb$	2σ	$^{208}Pb/^{232}Th$	2σ	$^{207}Pb/^{235}U$	2σ	$^{206}Pb/^{238}U$	2σ	$^{208}Pb/^{232}Th$	2σ	$^{207}Pb/^{206}Pb$	2σ
K2ZW8-01	696	527	114	0.76	0.61	0.019	0.0789	0.0019	0.0562	0.0016	0.02406	0.001	483	12	489	11	480	20	445	61
K2ZW8-02	338	236	45	0.70	0.616	0.041	0.0736	0.0017	0.0611	0.0043	0.02424	0.001	481	25	458	10	484	19	620	130
K2ZW8-03	800	407	83	0.51	0.61	0.022	0.0771	0.0014	0.057	0.0019	0.02264	0.0008	481	14	479	8.2	453	16	464	77
K2ZW8-04	840	497	103	0.59	0.64	0.025	0.0804	0.002	0.0561	0.0015	0.02365	0.0009	499	15	498	12	472	17	445	62
K2ZW8-05	800	564	123	0.71	0.7	0.1	0.081	0.0047	0.0593	0.0046	0.0271	0.0034	514	45	501	27	538	65	526	98
K2ZW8-06	1180	920	186	0.78	0.65	0.07	0.0735	0.0048	0.0627	0.0023	0.0243	0.0037	483	28	455	28	453	39	684	63
K2ZW8-07	514	470	99	0.91	0.594	0.025	0.072	0.0017	0.0594	0.0018	0.0224	0.0009	470	15	448	10	448	19	553	69
K2ZW8-08	550	383	76	0.70	0.574	0.024	0.0718	0.0019	0.0585	0.002	0.02158	0.0009	457	16	447	11	431	17	511	76
K2ZW8-09	406	287	55	0.71	0.601	0.027	0.0734	0.0015	0.0593	0.0022	0.0212	0.0009	475	17	457	9.1	424	18	561	82
K2ZW8-10	198	128	24	0.65	0.627	0.052	0.0735	0.0023	0.063	0.006	0.0243	0.0018	486	31	457	14	484	35	570	160

magmatic zircons (Belousova et al. 2002). The ages shown in Fig. 5 represent the weighted averages of the concordant and clustered $^{206}Pb/^{238}U$ ages of individual zircons. The results show that the data for the granite (K2-ZW8) plot on or near the Concordia line (Fig. 5a) and that the $^{206}Pb/^{238}U$ ages are distributed in the range from 447 to 501 Ma; the concordant U–Pb age is 468 ± 10 Ma (Fig. 5a) with a weighted mean age of 467 ± 13 Ma (n = 10, MSWD = 2.7) (Fig. 5b). The rare earth element (REE) results of zircons are shown in Table 2. The REE patterns show that zircons have typical igneous zircon features that are characterized by high HREE contents, conspicuous positive Ce anomalies, and negative Eu anomalies (Fig. 6).

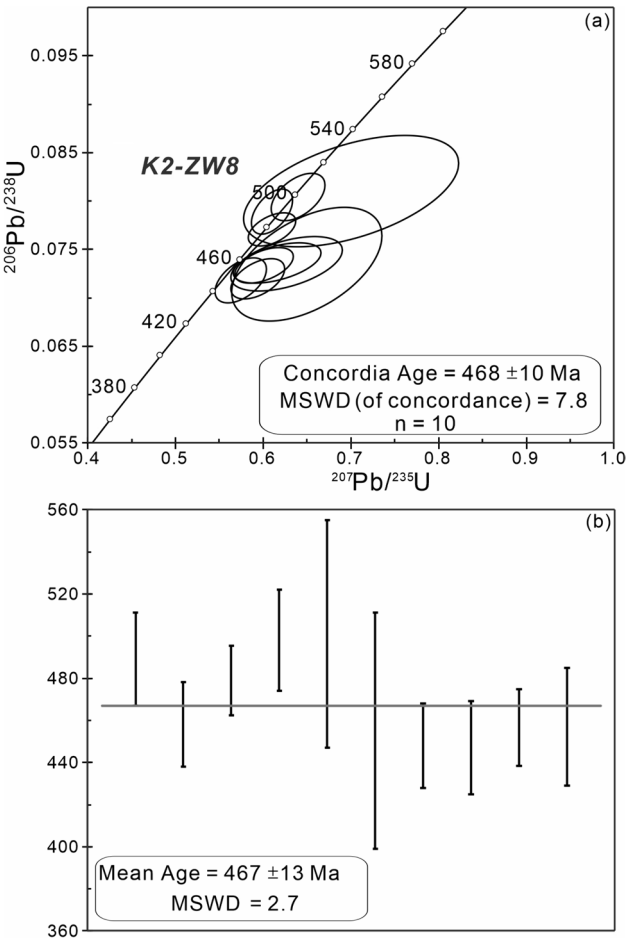

Fig. 5 Zircon U–Pb concordia age and mean age diagrams for the Beidaban granites

5.2 Whole-rock geochemistry

The major and trace element compositions of the granite samples in this study are listed in Table 3. Notably, one granite sample has a high K_2O content, which is probably caused by alteration because of its high loss on ignition (LOI). The contents of SiO_2, Al_2O_3, P_2O_5, and total alkalis ($K_2O + Na_2O$) range from 63.0wt% to 78.0wt%, 13.0wt% to 16.6wt%, 0.1wt% to 0.4wt%, and 7.1wt% to 9.2wt%, respectively, which indicate that the Beidaban granite is calc-alkaline, shoshonitic, and metaluminous (A/CNK = 0.7–0.9) (Fig. 7). The Lumanshan S/I-type granites (450 Ma, Zhao et al. 2022) exhibit geochemical characteristics similar to those of the Beidaban granites (Fig. 7). However, the whole-rock geochemical compositions of the postcollisional intrusions (alkali-feldspar granite, Zhang et al. 2017; quartz diorite, Fu et al. 2018; monzogranite, Wang et al. 2018) in the NQOB demonstrate that they are mostly subalkalic and medium- to high-K alkaline rocks with variable A/CNK ratios (Fig. 7).

The total REE (ΣREE) content in the Beidaban granite ranges from 215 to 530.0 μg/g, with an average of 325.1 μg/g. The light REE (LREE) contents are relatively high, ranging from 202.2 to 495.1 μg/g (302.3 on average), whereas the heavy REE (HREE) contents are relatively low, ranging from 12.4 to 34.5 μg/g (22.8 on average). The Beidaban granite shows negative europium anomalies (δEu = 0.5–0.8) in the chondrite-normalized pattern (Fig. 8a), with $(La/Yb)_N$ values ranging from 13.0 to 25.7. Except for 414 Ma A-type granites, most of the Paleozoic intrusions in the NQOB are characterized by small negative

Table 2 Rare earth element data of zircons from the Beidaban granites

Sample	La	Ce	Pr	Nd	Sm	Eu	Gd	Tb	Dy	Ho	Er	Tm	Yb	Lu
K2ZW8-01	0.11	36.2	0.12	1.41	3.25	0.782	19.1	6.26	76.1	28.6	132.6	28.2	277	58.1
K2ZW8-02	0.98	23.5	0.209	1.41	1.99	0.76	12	3.98	47.5	17.9	81.7	17.6	173	35
K2ZW8-03	0.44	22.5	0.079	0.72	1.68	0.383	9.72	3.85	47.9	19.54	95.8	22.9	231.9	52.1
K2ZW8-04	0.032	27.6	0.063	0.99	2.38	0.564	13.5	4.64	57.4	22.2	106	24	252	51.7
K2ZW8-05	2.15	66.8	3.59	20.1	21.3	15.9	40.1	12.1	141	42.9	186	41.9	484	74.3
K2ZW8-06	5.39	79.5	5.39	30.6	19.3	5.4	48.9	15.6	167	53.7	235	48.6	487	90.7
K2ZW8-07	10.7	47.8	2.33	11.5	6.78	2.33	27.2	7.85	85.5	31	141	30	289	63.5
K2ZW8-08	0.239	35.3	0.286	2.89	3.59	0.93	17.8	6.02	69.9	26.32	120.4	25.43	243.4	49.7
K2ZW8-09	0.196	27.8	0.118	1.5	2.68	0.74	14	4.74	53.9	20.7	95.9	20.8	219	43
K2ZW8-10	0.83	19.7	0.149	1.34	2.07	0.53	8.8	3.08	34	13.4	61.7	13.7	154	29.6

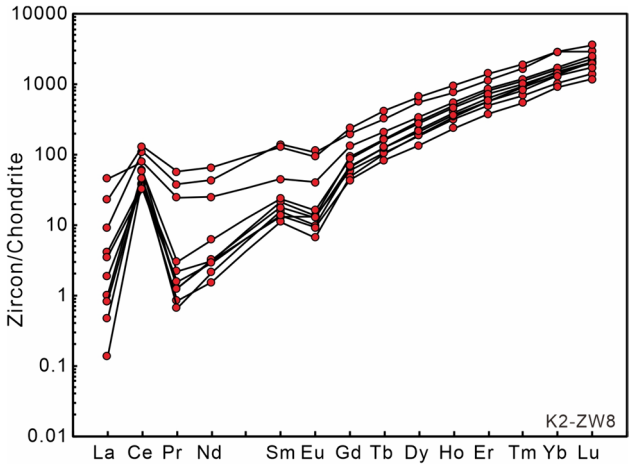

Fig. 6 Chondrite-normalized REE patterns for zircons from the Beidaban granites (normalizing data from Sun and McDonough 1989)

Eu anomalies in the REE distribution patterns (Fig. 8a–c). LREEs are generally enriched relative to HREEs, but the degree of enrichment varies among different Paleozoic intrusions. In the primitive mantle-normalized trace element diagram (Fig. 8d–f), the Beidaban and Lumanshan granites are enriched in large ion lithophile elements (LILEs; e.g., Rb, Th, Ba, K, and Sm) and depleted in high field strength elements (HFSEs; e.g., Nb, Ta, Ti, and Sr). The contents of Rb, Ba, Th, Sr, and P in the post-collisional intrusions (alkali-feldspar granite, quartz diorite, and monzogranite) are lower than those in the granites (Fig. 8f).

5.3 Sr–Nd and Pb isotopic compositions

The Sr–Nd isotopic compositions of the granite samples are given in Table 4. The Rb, Sr, Sm, and Nd values range from 195 to 302 μg/g, 165 to 473 μg/g, 5.4 to 14.9 μg/g, and 36.7 to 91.3 μg/g, respectively. The measured $^{87}Rb/^{86}Sr$, $^{87}Sr/^{86}Sr$, $^{147}Sm/^{144}Nd$, and $^{143}Nd/^{144}Nd$ values are 1.3280374–1.9620178, 0.717809–0.740767, 0.07867069–0.10503226, and 0.511751–0.512016, respectively. When the age of 468 Ma is used in the calculation, the initial $(^{87}Sr/^{86}Sr)_i$, $(^{143}Nd/^{144}Nd)_i$, and εNd(t) values vary from 0.70545 to 0.71082, 0.511478–0.511695, and − 10.9 to − 6.7, respectively. The calculated Nd isotope model ages (T_{DM}) and two-stage model ages (T_{DM2}) range from 1.49 to 1.80 Ga and from 1.74 to 2.08 Ga, respectively.

The Pb isotopic compositions are given in Table 5. The measured whole-rock $^{206}Pb/^{204}Pb$, $^{207}Pb/^{204}Pb$, and $^{208}Pb/^{204}Pb$ ratios are 19.89–21.93 (21.10 on average), 15.76–15.87 (15.82 on average), and 40.09–42.16 (40.83 on average), respectively. When the age of 468 Ma is used in the calculation, the initial $(^{206}Pb/^{204}Pb)$, $(^{207}Pb/^{204}Pb)$, and $(^{208}Pb/^{204}Pb)$ ratios are 19.14–20.26 (19.81 on average), 15.71–15.77 (15.75 on average), and 37.70–38.26 (38.01 on average), respectively.

6 Discussion

6.1 Petrogenesis and sources

The Beidaban granites and other Middle–Late Ordovician samples (> 450 Ma) in the NQOB are characterized by high contents of SiO_2 and K_2O and show metaluminous features (Fig. 7). In addition, euhedral primary hornblende, biotite, and Ti–Fe oxides frequently occur in the Beidaban granite (Fig. 3). These characteristics are indicative of I-type granite affinity (Miller 1985). The geochemical features of low A/CNK ratios (<1) (Fig. 7c), enrichment of LREEs and LILEs (Rb, Th, K), and depletion of HFSEs (Nb, Ta, Ti) (Fig. 8) also suggest that the Middle–Late Ordovician granites are likely arc I-type granitoids (Zhao et al. 2014). However, the Late Ordovician to Silurian granites (<440–438 Ma) are characterized by relatively low contents of SiO_2 and K_2O, high A/NK (Fig. 7), and low LREEs and Sr, P, and Ti (Fig. 8). In the FeOt/MgO vs. 10,000 * Ga/Al and Y vs. 10,000 * Ga/Al diagrams (Fig. 9a, b), nearly all the Early Paleozoic samples plot in the I-, and S-type fields except for several Late Silurian samples (414 Ma). These 414 Ma granites are A-type granitoids (Zhang et al. 2017) based on their major and trace element geochemical features (Figs. 7 and 8). The negative relationship between SiO_2 and P_2O_5 (Fig. 9c) suggests that the Beidaban granites and other Middle-Late Ordovician samples are I-type granites but that several Late Ordovician to Silurian granites are likely S-type granites. Nevertheless, some Beidaban granites also feature geochemical characteristics of S-type granites, such as relatively high contents of Al_2O_3 and K_2O. These characteristics are similar to those of the Lumanshan S/I-type granites (450 Ma, Zhao et al. 2022) in the NQOB. According to the ACF classification diagram (Fig. 9d), most of the samples from Beidaban granites and Middle-Late Ordovician granites plot in the S-type field, whereas most of the Silurian granite samples (<434 Ma) plot in the I-type field. Significantly, some of the Beidaban samples in this study straddle the boundary between S-type and I-type granitoids. Therefore, recent studies suggested that these types of granites do not belong to pure I-type granites because of their multiple melt sources (called transitional I/S-type granites) (Chappell et al. 2012; Gao et al. 2016; Wang et al. 2018; Zhao et al. 2022). Thus, based on the above discussions, we propose that the Beidaban granites probably represent transitional I/S-type granitoids.

The nearly equal Sr and Nd isotopic values (Table 4) of the Beidaban granites suggest that they were cogenetic.

Table 3 Major element (wt.%) and trace element (ug/g) compositions of the Beidaban granites

Sample	SiO_2	Al_2O_3	Fe_2O_3	CaO	MgO	K_2O	Na_2O	TiO_2	P_2O_5	MnO	LOI	Total	FeO_{Total}	K_2O/Na_2O	A/CNK	A/NK	Sc	V
K2-ZW6	62.95	16.56	3.66	2.07	1.10	6.46	2.70	0.33	0.14	0.11	3.47	99.56	4.96	2.39	0.85	1.45	10.80	50.10
K2-ZW7	67.76	13.26	3.95	2.23	1.54	4.65	2.64	0.50	0.26	0.13	3.00	99.91	5.78	1.76	0.78	1.41	11.20	82.10
K2-ZW8	67.32	13.43	3.85	2.48	1.74	4.97	2.51	0.45	0.25	0.08	2.86	99.93	5.77	1.98	0.75	1.41	9.36	69.30
K2-ZW9	67.96	12.99	3.97	2.45	1.76	4.82	2.26	0.50	0.32	0.07	2.78	99.88	5.89	2.13	0.75	1.45	8.35	72.60
K2-ZW10	69.95	13.93	3.03	1.36	1.14	5.18	2.78	0.35	0.16	0.07	1.94	99.89	4.04	1.86	0.90	1.37	6.08	52.00
K2-ZW11	65.34	14.05	4.54	2.52	1.88	5.67	2.45	0.53	0.35	0.09	2.44	99.85	6.32	2.31	0.70	1.38	10.50	87.10
Sample	Cr	Co	Ni	Ga	Rb	Sr	Y	Cs	Ba	La	Ce	Pr	Nd	Sm	Eu	Gd	Tb	Dy
K2-ZW6	9.86	4.65	4.31	19.10	302.00	165.00	28.70	4.16	722.00	74.60	134.00	13.00	46.50	8.14	1.66	6.61	1.12	6.90
K2-ZW7	16.60	12.10	8.04	18.10	213.00	348.00	40.00	3.81	653.00	136.00	225.00	25.70	91.30	14.90	2.16	10.50	2.02	11.30
K2-ZW8	18.80	10.10	8.80	15.80	228.00	337.00	23.80	2.65	903.00	70.60	126.00	15.00	54.60	7.98	1.78	6.88	1.15	6.36
K2-ZW9	15.80	11.70	9.13	16.00	195.00	384.00	26.90	2.85	990.00	55.00	85.00	13.10	50.80	8.76	1.91	7.17	1.25	6.64
K2-ZW10	10.30	6.95	4.35	17.90	252.00	473.00	12.70	5.35	703.00	61.90	87.00	9.84	36.70	5.45	1.33	4.01	0.71	3.42
K2-ZW11	23.00	12.10	10.00	15.30	196.00	428.00	26.90	4.02	1237.00	97.40	157.00	17.00	66.20	8.68	1.76	8.50	1.25	6.19
Sample	Ho	Er	Tm	Yb	Lu	Th	U	Nb	Ta	Zr	Hf	ΣREE	LREE	HREE	LREE/HREE	LaN/YbN	δEu	δCe
K2-ZW6	1.01	2.71	0.51	3.41	0.45	52.10	10.70	19.50	1.73	145.00	4.55	300.62	277.90	22.72	12.23	15.69	0.67	0.97
K2-ZW7	1.34	3.71	0.73	4.31	0.54	63.40	7.37	35.50	2.95	149.00	4.63	529.51	495.06	34.45	14.37	22.63	0.50	0.87
K2-ZW8	0.77	2.53	0.44	2.72	0.32	46.00	5.67	20.40	1.84	128.00	3.88	297.14	275.96	21.18	13.03	18.62	0.72	0.90
K2-ZW9	0.94	2.83	0.50	3.03	0.34	43.90	4.59	22.10	1.69	105.00	2.89	237.27	214.57	22.70	9.45	13.02	0.71	0.75
K2-ZW10	0.57	1.52	0.28	1.73	0.21	29.80	6.00	16.90	1.71	124.00	3.53	214.66	202.22	12.44	16.26	25.67	0.83	0.78
K2-ZW11	1.00	2.79	0.48	2.88	0.39	49.10	6.93	21.50	1.83	130.00	4.13	371.51	348.04	23.47	14.83	24.26	0.62	0.87

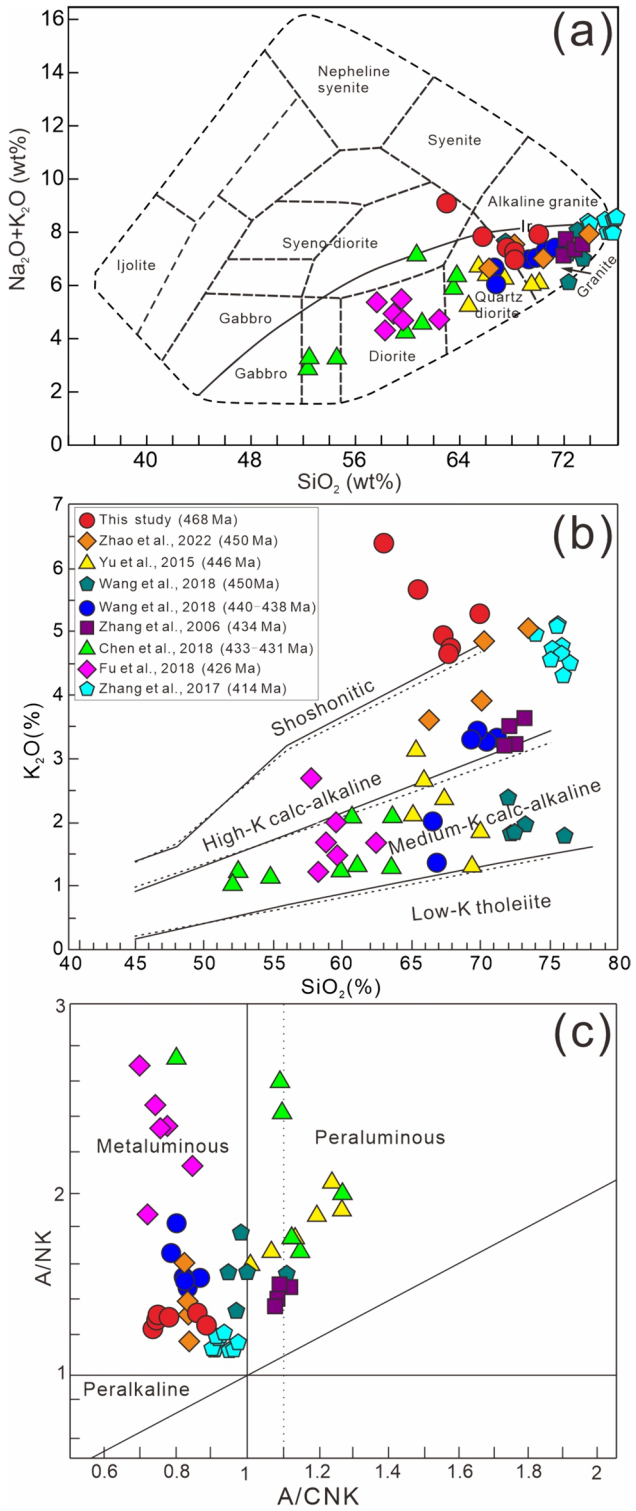

Fig. 7 K_2O+Na_2O vs. SiO_2 (**a**, modified from Middlemost 1994), K_2O vs. SiO_2 (**b**, modified from Peccerillo and Taylor 1976), and A/NK vs. A/CNK (**c**, modified from Maniar and Piccoli 1989) classification diagrams of the Beidaban granites. Legends of cited data from the NQOB in Figs. 9, 10, 11 and 12 are the same as in this figure

Generally, crustal melts have negative εNd(t) values and high initial $(^{87}Sr/^{86}Sr)i$ values, whereas mantle magmas have positive εNd(t) values along the mantle array (Kinny and Maas 2003). The high initial $(^{87}Sr/^{86}Sr)_i$ values (0.70545–0.71082) and negative εNd(t) values (-10.9 to -6.7) strongly indicate that continental crust was involved in the genesis of the Beidaban granite. In the εNd(t) vs. t(Ga) diagram (Fig. 10a), the Beidaban granites plot in Paleo-Mesoproterozoic crustal field, indicating that they were generated by melting of the Paleo-Mesoproterozoic crustal basement and were probably caused by magma underplating (Huang et al. 2015; Zhu et al. 2022). As illustrated in Fig. 10b, although the Beidaban granites overlap the field of Paleozoic granitoids in Qilian, they plot in the lower left field of I-type granitoids. This means that the magma sources for the Beidaban granites were different from those for the I-type granitoids in Qilian and were more likely derived from Paleo-Mesoproterozoic continental crustal material (Chu et al. 2006; Zhou et al. 2017; Yang et al. 2018). This explanation is supported by the two-stage Nd model ages (T_{DM2}) of 1.74–2.08 Ga. Similar cases are observed for the Lumanshan granites (450 Ma, Zhao et al. 2022) in the NQOB (Fig. 10b). However, the high εNd(t) values and low initial $(^{87}Sr/^{86}Sr)$ values (Fig. 10a, b) suggest that the 446 Ma granites were generated by partial melting of thickened crust (Yu et al. 2015). Compared to those of the Beidaban granites, the 440–438 Ma, 434 Ma, and 433–431 Ma granitoids in the NQOB have higher εNd(t) values and lower initial $(^{87}Sr/^{86}Sr)i$ values (Fig. 10b), which are indicative of mantle isotopic signatures or material evidence of melting ocean crust (Zhang et al. 2006; Chen et al. 2018; Wang et al. 2018). The 414 Ma granites are possibly derived from partial melting of felsic crustal material, which was caused by lithospheric delamination after the collision (Zhang et al. 2017). The Pb isotope values, which plot in the field of continental crust and above the Northern Hemisphere Reference Line (NHRL) in the $(^{206}Pb/^{204}Pb)$ vs. $(^{207}Pb/^{204}Pb)$ diagram (Fig. 10c), suggest continental crust source for the Beidaban granite. In addition, geochemical features such as high Th/Ta (17.43–30.12) and Rb/Nb (6.01–15.49), which are obviously greater than those of the continental crust (Rudnick and Gao 2003), are also consistent with a recycled crustal component (Taylor and Mclennan 1985).

Studies reveal that dehydration melting of metapelites and metagreywackes yields higher $Al_2O_3/(TFeO+MgO+TiO_2)$ and lower $CaO+TFeO+MgO+TiO_2$ values compared to that of metabasaltic rocks (Kaygusuz et al. 2008). Melting experiments also reveal that melting products of mafic lower crust yield lower K_2O/Na_2O, Rb/Ba, and Rb/Sr ratios and $Al_2O_3/(MgO+TFeO)$ contents or higher $Al_2O_3+TFeO+MgO+TiO_2$ contents compared to those of metasedimentary rocks (Rushmer 1991; Patiño Douce and Beard 1996; Kaygusuz et al. 2008). Thus, the

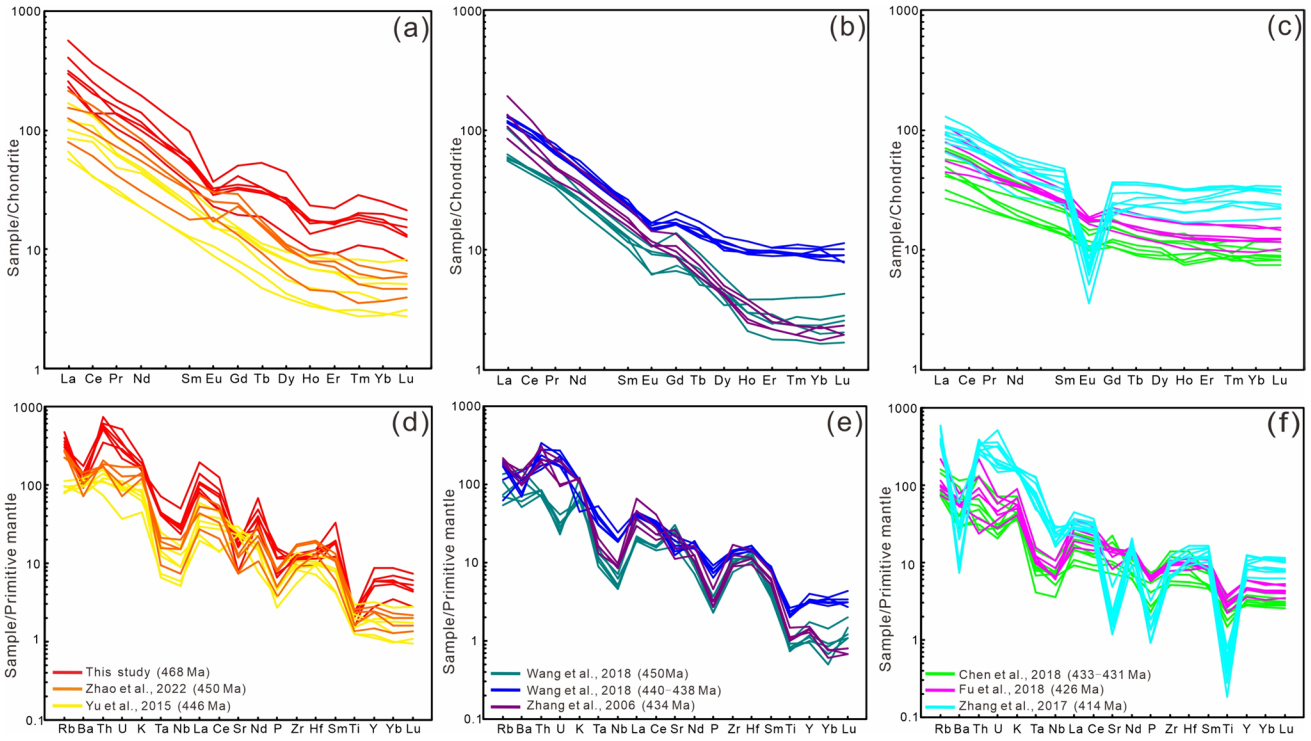

Fig. 8 Chondrite-normalized rare-earth element patterns (**a**, **b**, **c**) and primitive mantle-normalized trace element patterns (**d**, **e**, **f**) for the Beidaban granites and other cited data in the NQOB. Chondrite values and primitive mantle values are from Sun and McDonough (1989)

Table 4 Sr and Nd isotopic data and calculated values for the Beidaban granites

Sample	Rb	Sr	Sm	Nd	$^{87}Rb/^{86}Sr$	$^{87}Sr/^{86}Sr$	$^{147}Sm/^{144}Nd$	$^{143}Nd/^{144}Nd$	$(^{87}Sr/^{86}Sr)i$	εNd(t)	T_{DM} (Ma)	T_{DM2} (Ma)
K2-ZW6	302	165	8.14	46.5	5.307879	0.740767	0.105032	0.512016	0.705451366	−6.67	1590	1742
K2-ZW7	213	348	14.9	91.3	1.775015	0.720307	0.097919	0.511929	0.70849715	−7.96	1607	1845
K2-ZW8	228	337	7.98	54.6	1.962018	0.721477	0.087692	0.511885	0.708422839	−8.19	1530	1865
K2-ZW9	195	384	8.76	50.8	1.472656	0.720617	0.103465	0.511842	0.710818775	−9.97	1807	2009
K2-ZW10	252	473	5.45	36.7	1.545032	0.718646	0.089101	0.511751	0.70836623	−10.9	1710	2084
K2-ZW11	196	428	8.68	66.2	1.328037	0.717809	0.078671	0.511822	0.708972988	−8.89	1499	1921

Table 5 Pb isotopic data and initial ratios for the Beidaban granites

Sample	Pb	Th	U	$^{208}Pb/^{204}Pb$	$^{207}Pb/^{204}Pb$	$^{206}Pb/^{204}Pb$	$(^{206}Pb/^{204}Pb)t$	$(^{207}Pb/^{204}Pb)t$	$(^{208}Pb/^{204}Pb)t$
K2-ZW6	37.9	52.1	10.7	40.356	15.816	20.968	19.5357	15.7352	38.114
K2-ZW7	49.5	63.4	7.37	40.095	15.761	19.89	19.1481	15.7192	38.0434
K2-ZW8	32.6	46	5.67	40.565	15.805	20.745	19.8629	15.7552	38.2644
K2-ZW9	21.4	43.9	4.59	41.092	15.823	21.244	20.1417	15.7608	37.7027
K2-ZW10	18.7	29.8	6	40.747	15.865	21.925	20.2681	15.7715	38.1015
K2-ZW11	19.3	49.1	6.93	42.164	15.867	21.841	19.9556	15.7607	37.8698

Beidaban granites and the 450 Ma granites with relatively high K_2O/Na_2O, Rb/Ba, and Rb/Sr ratios and low $Al_2O_3 + TFeO + MgO + TiO_2$ contents are thought to be mainly derived from metasedimentary rocks, which is consistent with the plot of the Rb/Sr vs. Rb/Ba diagram (Fig. 11a). However, scholars have proposed that the CaO/Na_2O ratios of felsic rocks derived from partial melting of metagraywackes and igneous sources range from

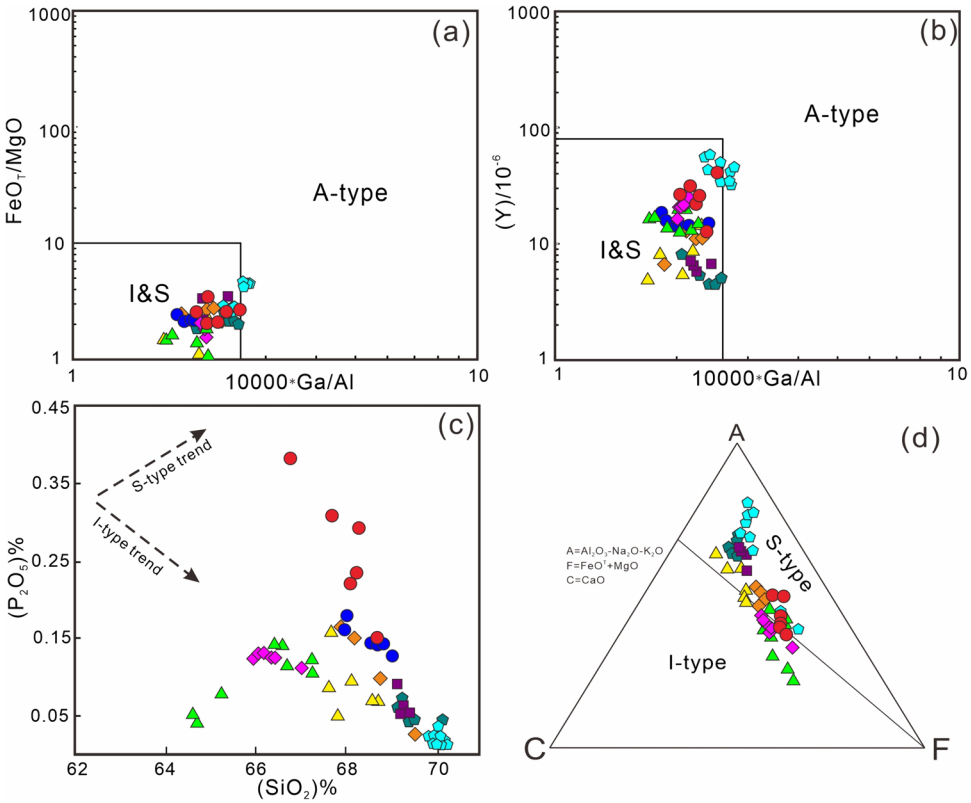

Fig. 9 Whole-rock major and trace element discrimination diagrams for the Beidaban granites. **a** FeOt/MgO vs. 10 000×Ga/Al; **b** Y vs. 10,000×Ga/Al; **c** SiO_2 vs. P_2O_5; **d** A-C-F. **a** and **b** are modified from Whalen et al. (1987); **d** is modified from Lameyre and Bowden. (1982)

0.3 to 1.5 (Jung and Pfänder 2007; Sylvester 1998). The high CaO/Na_2O ratios (0.49–1.08) of the Beidaban granites and the 450 Ma granites are supposed to indicate the partial melting of metagraywackes and igneous sources. Furthermore, the CaO/Na_2O vs. CaO/TFeO diagram suggests metagraywacke and granitoid sources for the Beidaban granites (Fig. 11b). Robust persuasiveness cannot be founded upon a single discriminant diagram. In the discriminant diagrams of $Al_2O_3 + TFeO + MgO + TiO_2$ vs. $Al_2O_3/(TFeO + MgO + TiO_2)$ and molar $CaO/(MgO + TFeO)$ vs. molar $Al_2O_3/(MgO + TFeO)$, the Beidaban granites and the 450 Ma granites plot not only in the field of partial melting of metagraywacke sources but also in amphibolites or metabasaltic to metatonalitic sources (Fig. 11c, d). Therefore, it is reasonable to confirm that the transitional I/S-type Beidaban granites and the 450 Ma granites were derived from heterogeneous magma sources produced by partial melting of metagreywackes and igneous rocks (Sylvester 1998; Altherr and Siebel 2002; Kaygusuz et al. 2008).

6.2 Tectonic implications

Zircon geochronology studies of intermediate-acidic igneous rocks in the NQOB imply that these igneous rocks span a long history of tectonic evolution between 853 and 211 Ma (Zhu et al. 2022 and references therein). Paleozoic igneous rocks, especially Early Paleozoic granitoids, are distributed in the NQOB, and geochronological and geochemical studies on these granitoids indicate that continental breakup (680–520 Ma) and development of the Paleo Qilian Ocean (520–495 Ma) occurred in the NQOB (Xia et al. 1999; Xiao et al. 2009; Zhang et al. 2012). Although controversies regarding the subduction polarity of the North Qilian Ocean exist (Zhang et al. 1997, 2012; Xia et al. 2003), north-dipping subduction along the northern margin of the QOB during the early Paleozoic has been accepted by most scholars (Song et al. 2013; Xia et al. 2016; Zhu et al. 2022). However, despite previous studies on Paleozoic granites in the NQOB (Xia et al. 2012; Zhang et al. 2017; Yang et al. 2018; Wang et al. 2018; Fu et al. 2018; Zhao et al. 2022), the important first-order problems related to the transitional tectonic setting (from arc to initial collision) or the initial closure timing of the North Qilian Ocean have been poorly constrained, which limits the ability to reconstruct the tectonic mechanism of magma generation in the NQOB. Therefore, the Middle Ordovician to Silurian granitoids with ages ranging from

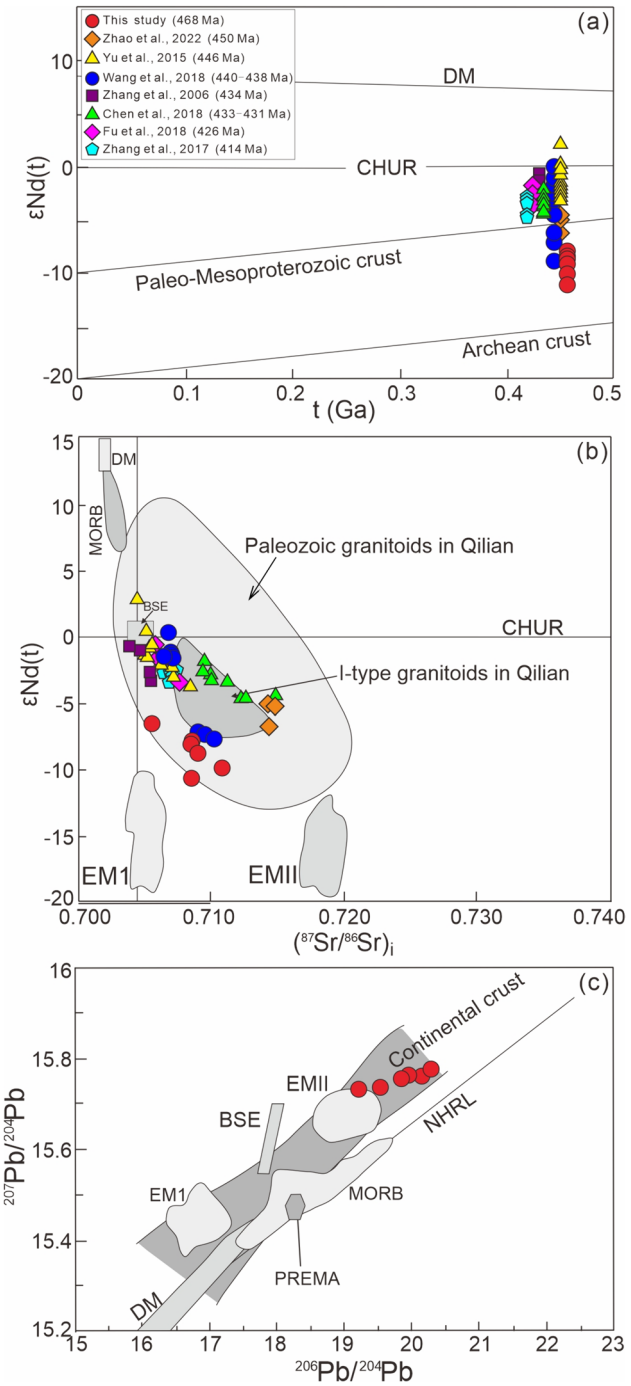

Fig. 10 Sr, Nd, and Pb isotopic composition and ratios for the Beidaban granites and other cited data in the NQOB. **a** εNd(t) vs. t (Ga) diagram. **b** εNd(t) vs. $(^{87}Sr/^{86}Sr)_i$ diagram (modified from Zindler and Hart 1986). Fields for Paleozoic granitoids and I-type granitoids in Qilian are based on Zhu et al. (2022) and Zhang et al. (2017). **c** ($^{206}Pb/^{204}Pb$) vs. ($^{207}Pb/^{204}Pb$) diagram. Data of EM I, EM II, BSE, MORB, and NHRL are from Zindler and Hart (1986); continental crust data from Zartman and Doe (1981)

468 to 414 Ma that occurred in the NQOB are summarized for comparison.

As mentioned above, the Beidaban granites yield a zircon U–Pb age of 468 ± 10 Ma and contain K-feldspar, amphibole, biotite, and Ti–Fe oxides with A/CNK values less than 1, which illustrates that they are K-rich porphyritic calc-alkaline granitoids (KCGs). This type of granitoid is indicative of an initial collisional setting (Barbarin 1999). However, the transitional I/S-type Beidaban granites and the Middle Ordovician granites (> 446 Ma) also show geochemical characteristics similar to those of adakitic island-arc-type granitoids (Fig. 12a). Based on these findings, we suggest that the transition from subduction to collision environment in the NQOB probably did not occur earlier than 468 Ma. Previous studies proposed that the North Qilian Ocean closed before 450 Ma (Zhao et al. 2022). In the Yb + Ta vs. Rb and Y vs. Nb diagrams, nearly all the Beidaban granites and Middle-Late Ordovician granites (> 446 Ma) plot in the fields of VAG and Syn-COLG (Fig. 12b, c), indicating that they likely represent the products of final arc and incipient syncollisional magmatism (Sylvester 1998). These geochronological and geochemical features provide significant information about tectonic processes after the closure of the North Qilian Ocean (Yu et al. 2015). As the North Qilian Ocean closed, the island arc crust was considerably shortened and thickened, and the syn-collisional magmatism in the NQOB contributed to continental crust growth (Zhang et al. 2006; Chen et al. 2018; Fu et al. 2018). Several recent studies proposed that the NQOB featured a collisional setting at ca. 442–422 Ma (Wu et al. 2010; Song et al. 2013; Zhang et al. 2017; Li et al. 2017; Wang et al. 2018; Zhao et al. 2022), as evidenced by the Qingshan monzogranite (440–438 Ma), Laohushan quartz diorites (426 Ma), and Shengrongsi granites (422 Ma). These granites are distributed mainly in the conjunction area between the NQOB and the Alxa block and have geological and geochemical features related to the compressional environment generated by the collision between the Qilian-Qaidam block and the Alxa block (Fu et al. 2018). Comparatively, the 414 Ma A-type granites are different from the island-arc-type and syn-collisional granites in the NQOB (Fig. 12). These A-type magmatic suites were post-collisional granites and were probably generated by lithospheric delamination after the collision (Zhang et al. 2017). Therefore, based on our work and previous studies, we propose that the Beidaban granites record the tectonic transition setting from subduction in the Qilian Ocean to initiation of collision and that the final closure of the Qilian Ocean

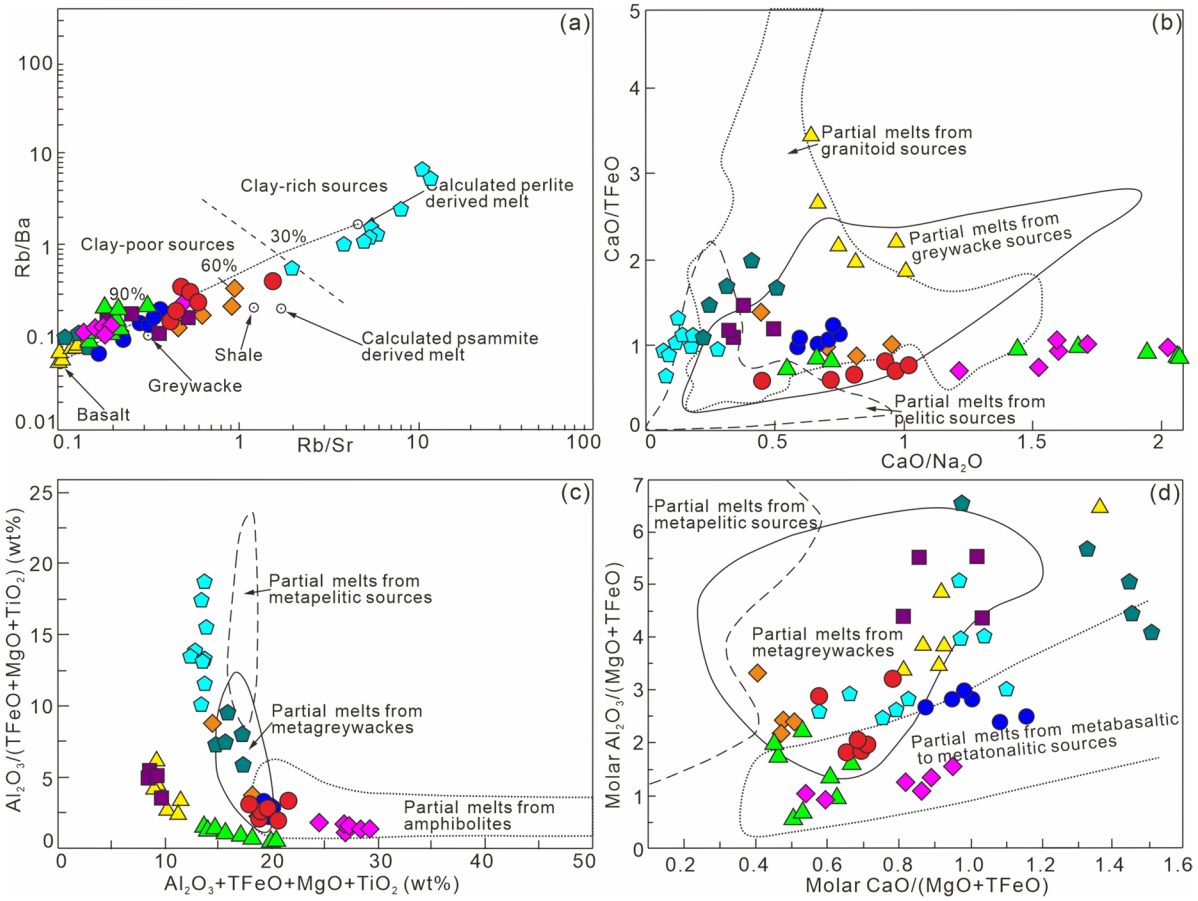

Fig. 11 Major and trace element discrimination diagrams for the Beidaban granites. **a** Rb/Sr vs. Rb/Ba (modified from Sylvester 1998). **b** CaO/Na_2O vs. CaO/TFeO (modified from Yang et al. 2016). **c** $Al_2O_3+TFeO+MgO+TiO_2$ vs. $Al_2O_3/(TFeO+MgO+TiO_2)$ (modified from Kayguzuz et al. 2008). **d** molar CaO/(MgO + TFeO) vs. molar Al_2O_3/(MgO + TFeO) (modified from Altherr et al. 2000)

can be constrained to the Middle–Late Ordovician (ca. 468–450 Ma).

7 Conclusions

(1) Zircon U–Pb ages show that the Beidaban granite were emplaced at 468 ± 10 Ma, indicating Middle Ordovician magmatism in the central part of the North Qilian Orogenic Belt.

(2) The Beidaban granites contain amphibole, biotite, and Ti–Fe oxides and are K-rich porphyritic calc-alkaline granitoids. The geochemical characteristics indicate that the Beidaban granites represent transitional I/S-type granitoids.

(3) The high initial $(^{87}Sr/^{86}Sr)_i$ values (0.70545–0.71082), clearly negative εNd(t) values (− 10.9 to − 6.7), and high initial Pb isotopic compositions ($^{206}Pb/^{204}Pb = 19.14–20.26$; $^{207}Pb/^{204}Pb = 15.71–15.77$) suggest that the Beidaban granites originated from recycled crustal components and were probably derived from partial melting of a metasedimentary source with the involvement of igneous rocks.

(4) The timing of the tectonic transition in the NQOB from an arc to a collisional setting and the final closure of the Qilian Ocean can be constrained to the Middle-Late Ordovician (ca. 468–450 Ma).

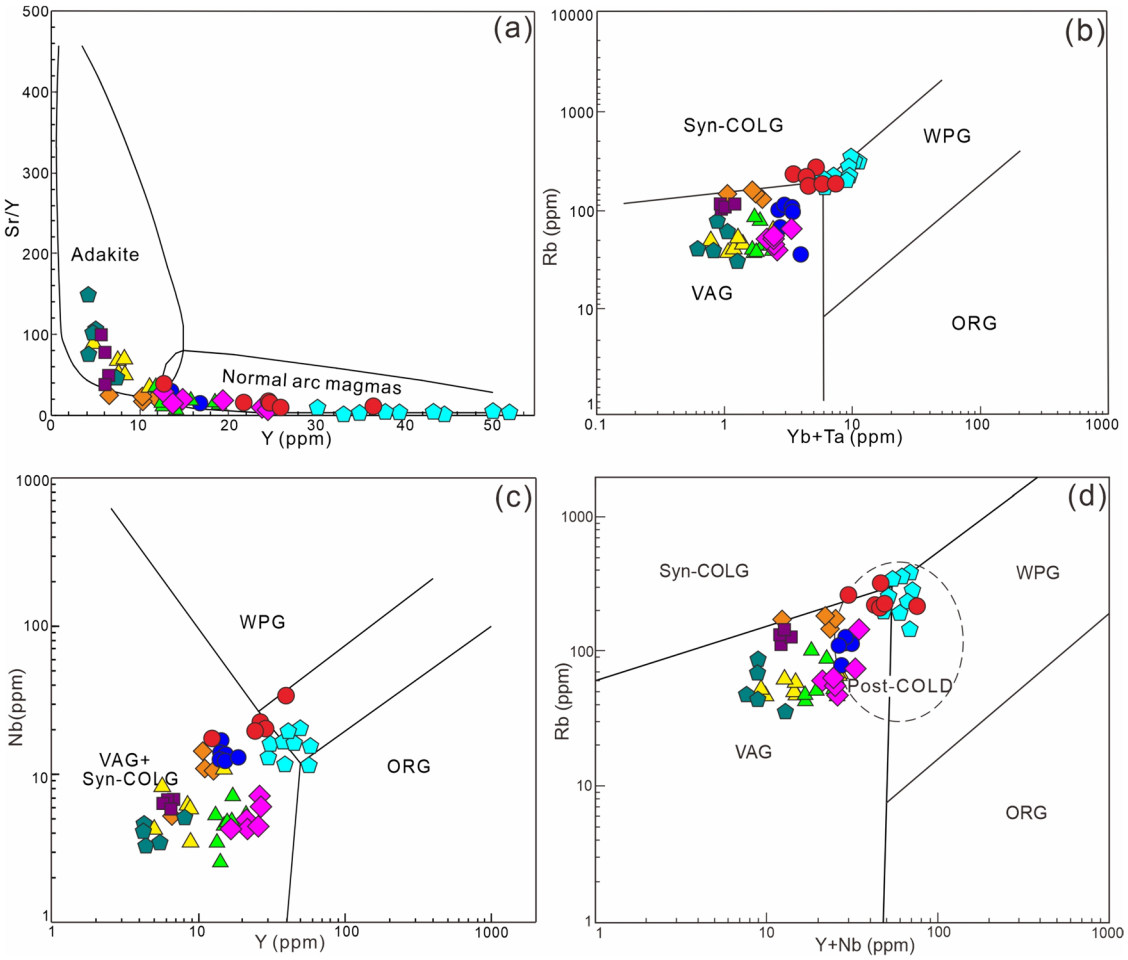

Fig. 12 Discrimination diagrams for the Beidaban granites. **a** Y vs. Sr/Y (modified from Drummond and Defant 1990). **b** Yb + Ta vs. Rb. **c** Y vs. Nb. **d** Y + Nb vs. Rb. Normalization values of **b**, **c**, and **d** are from Pearce et al. (1984). ORG: ocean ridge granites; VAG: volcanic arc granites; WPG: within plate granites; COLG: collision granites

Acknowledgements This study was financially supported by the Youth Science and Technology Talent Recruitment Project of Gansu Province (2022–19), and Technological Innovation Project of Gansu Provincial Department of Natural Resources (2022–3, 2022–4, 2022–28), National Natural Science Foundation of China (Nos. 42073059 and 42303034), Outstanding Youth Fund of Anhui Provincial Department of Education (No. 2022AH020084), and Doctoral Startup Foundation of Suzhou University (2021BSK038). The authors would like to thank Yonggang Sun, Wei Tao, and Shisheng Li for their contribution that made this work better. We thank three anonymous reviewers for their critical reviews and constructive comments, which significantly improved the manuscript.

Author contributions Zhi-yuan Sun designed the study. Tao Yang performed the data analysis. Tao Yang and Zhi-yuan Sun wrote the manuscript. Ming-liang Wang, Xiao-qiang Zhu, and Jing-yu Zhao guided us safely and enthusiastically through the field and experiment process.

Funding This study was financially supported by the Youth Science and Technology Talent Recruitment Project of Gansu Province (2022–19), and Technological Innovation Project of Gansu Provincial Department of Natural Resources (2022–3, 2022–4, 2022–28), National Natural Science Foundation of China (Nos. 42073059 and 42303034), Outstanding Youth Fund of Anhui Provincial Department of Education (No. 2022AH020084), and Doctoral Startup Foundation of Suzhou University (2021BSK038).

Declarations

Conflict of interest All the authors declare that the manuscript has not been submitted to more than one journal for simultaneous consideration. The manuscript has not been published previously. No data have been fabricated or manipulated (including images) to support our conclusions. Consent to submit has been received from all co-authors and responsible authorities at the institute/organization where the work has been carried out before the work is submitted. Authors whose names appear on the submission have contributed sufficiently to the scientific work and therefore share collective responsibility and accountability for the results. We understand that the corresponding author is responsible for communicating with the other authors about progress, submissions of revisions and final approval of proofs. The authors declare that they have no competing interests or conflict of interest.

References

Altherr R, Holl A, Hegner E, Langer C, Kreuzer H (2000) High-potassium, calc-alkaline I-type plutonism in the European Variscides: Northern Vosges (France) and northern Schwarzwald (Germany). Lithos. 50:51–73. https://doi.org/10.1016/S0024-4937(99)00052-3

Altherr R, Siebel W (2002) I-type plutonism in a continental back-arc setting: Miocene granitoids and monzonites from the central Aegean Sea, Greece. Contrib Mineral Petrol. 143:397–415. https://doi.org/10.1007/s00410-002-0352-y

Barbarin B (1999) A review of the relationships between granitoid types, their origins and their geodynamic environments. Lithos. 46:605–626. https://doi.org/10.1016/S0024-4937(98)00085-1

Belousova EA, Griffin WL, Oreilly SY, Fisher N (2002) Igneous zircon: Trace element composition as an indicator of source rock type. Contrib Mineral Petrol. 143:602–622. https://doi.org/10.1007/s00410-002-0364-7

Chappell BW, White AJR (1974) Two contrasting granite types. Pac Geol. 8:173–174. https://doi.org/10.1046/j.1440-0952.2001.00882.x

Chappell BW, Bryant CJ, Wyborn D (2012) Peraluminous I-type granites. Lithos. 153:142–153. https://doi.org/10.1016/j.lithos.2012.07.008

Chen S, Niu YL, Xue QQ (2018) Syn-collisional felsic magmatism and continental crust growth: A case study from the North Qilian Orogenic Belt at the northern margin of the Tibetan Plateau. Lithos. 308–309:53–64. https://doi.org/10.1016/j.lithos.2018.03.001

Chen YJ, Yang K, Wu B, Zhao RY, Wang G, Gou XM (2019) Zircon U-Pb dating and its geological implications in Beidaban granite, Northern Qilian, Gansu Province. J East China Univ Tech (Nat Sci). 42:108–115 (**in Chinese with English abstract**).

Cheng H, Lu T, Cao D (2016) Coupled Lu-Hf and Sm-Nd geochronology constrains blueschist-facies metamorphism and closure timing of the Qilian Ocean in the North Qilian orogeny. Gondwana Res. 34:99–108. https://doi.org/10.1016/j.gr.2016.03.008

Chu MF, Chung SL, Song B, Liu DY, O'Reilly SY, Pearson NJ, Wen DJ (2006) Zircon U-Pb and Hf isotope constraints on the Mesozoic tectonics and crustal evolution of southern Tibet. Geology. 34:745–748. https://doi.org/10.1130/G22725.1

Clemens JD (2003) S-type granitic magmas—petrogenetic issues, models and evidence. Earth Sci Rev. 61:1–18. https://doi.org/10.1016/S0012-8252(02)00107-1

Drummond MS, Defant MJ (1990) A model for trondhjemite–tonalite–dacite genesis and crustal growth via slabmelting: Archean to modern comparisons. J Geophys Res. 95:21503–21521. https://doi.org/10.1029/JB095iB13p21503

Fu D, Kusky T, Wilde SA, Polat A, Huang B, Zhang ZP (2018) Early Paleozoic collision-related magmatism in the eastern North Qilian orogen, northern Tibet: a linkage between accretionary and collisional orogenesis. Geol Soc Am Bull. 113:1031–1056. https://doi.org/10.1130/B35009.1

Gao P, Zheng YF, Zhao ZF (2016) Distinction between S-type and peraluminous I-type granites: Zircon versus whole-rock geochemistry. Lithos. 258–259:77–91. https://doi.org/10.1016/j.lithos.2016.04.019

Gao XY, Yu SY, Peng YB, Lv P, Wang M, Liu YJ, Li SZ, Jiang XZ, Ji WT, Li CZ (2021) Insights into OIB-like magmatism contemporaneous with oceanic subduction: petrogenetic constraints on the Kendelong metagabbro in the North Qaidam. Lithos. 392–393:106130. https://doi.org/10.1016/j.lithos.2021.106130

He SX, Tang SH, Zhu XK, Wang JH (2007) Precise measurement of Nd isotopic ratios by means of multi-collector magnetic sector inductively coupled plasma mass spectrometry. Acta Geosci Sin. 28:405–410 (**in Chinese with English abstract**).

He SX, Zhu XK, Yang C, Tang SH (2005) High-precision analysis of Pb isotope ratios using MC-ICPMS. Acta Geosci Sin. 26:19–22 (**in Chinese with English abstract**).

Hopkinson TN, Harris NBW, Warren CJ, Spencer CJ, Roberts NMW, Horstwood MSA, Parrish RR (2017) The identification and significance of pure sediment-derived granites. Earth Planet Sci Lett. 467:57–63. https://doi.org/10.1016/j.epsl.2017.03.018

Huang H, Niu YL, Nowell G, Zhao ZD, Yu XH, Mo XX (2015) The nature and history of the Qilian Block in the context of the development of the Greater Tibetan Plateau. Gondwana Res. 28:209–224. https://doi.org/10.1016/j.gr.2014.02.010

Jung S, Pfänder JA (2007) Source composition and melting temperatures of orogenic granitoids: Constraints from CaO/Na_2O, Al_2O_3/TiO_2 and accessory mineral saturation thermometry. Eur J Mineral. 19:859–870. https://doi.org/10.1127/0935-1221/2007/0019-1774

Kaygusuz A, Siebel W, Sen C, Satir M (2008) Petrochemistry and petrology of I-type granitoids in an arc setting: The composite Torul pluton, Eastern Pontides, NE Turkey. J Earth Sci. 97:739–764. https://doi.org/10.1007/s00531-007-0188-9

Kinny PD, Maas R (2003) Lu–Hf and Sm–Nd isotope systems. Earth Planet Sci Lett. https://doi.org/10.1016/S0012-821X(99)00047-3

Lameyre J, Bowden P (1982) Plutonic rock types series: Discrimination of various granitoid series and related rocks. J Volcanol Geotherm Res. 14:169–186. https://doi.org/10.1016/0377-0273(82)90047-6

Li SZ, Yang Z, Zhao SJ, Li XY, Guo LL, Yu S, Lan HY (2016) Global Early Paleozoic orogens (I), collision-type orogeny. J Jilin Univ (Earth Sci Ed). 46:945–967 (**in Chinese with English abstract**).

Li SZ, Jahn BM, Zhao SJ, Dai LM, Li XY, Suo YH, Wang PC (2017) Triassic southeastward subduction of North China block to South China block: Insights from new geological, geophysical and geochemical data. Earth Sci Rev. 166:270–285. https://doi.org/10.1016/j.earscirev.2017.01.009

Li YL, Tong X, Zhu YH, Lin JW, Zheng JP, Brouwer FM (2018) Tectonic affin- ity and evolution of the Precambrian Qilian block: insights from petrology, geo-chemistry and geochronology of the Hualong Group in the Qilian Orogen, NW China. Precambrian Res. 315:179–200. https://doi.org/10.1016/j.precamres.2018.07.025

Li YL, Xiao WL, Zheng JP, Brouwer FM (2022) Northward subduction of the South Qilian ocean: Insights from Early Paleozoic magmatism in the South-Central Qilian belts. Geosy Geoenviron. 100013:1–10.

Lin YH, Zhang LF, Ji JQ, Song SG (2010) $^{40}Ar/^{39}Ar$ age of Jiugequan lawsonite blueschists in northern Qilian Mountains and its petrologic significance. Chin Sci Bull. 5:2021–2027. https://doi.org/10.1007/s11434-010-3239-8

Liu CF, Wu C, Zhou ZG, Yan Z, Jiang T, Song ZJ, Liu WC, Yang X, Zhang HY (2018) U-Pb detrital zircon geochronology from the basement of the Central Qilian Terrane: implications for tectonic evolution of northeastern Tibetan Plateau. Int J Earth Sci. 107:673–686. https://doi.org/10.1007/s00531-017-1522-5

Liu YS, Hu ZC, Gao S, Günther D, Xu J, Gao CG, Chen HH (2008) In-situ analysis of major and trace elements of anhydrous minerals by LA-ICP-MS without applying an internal standard. Chem Geol. 257:34–43. https://doi.org/10.1016/j.chemgeo.2008.08.004

Ludwig KR (2003) Using ISOPLOT/Ex: a geochronological toolkit for Microsoft excel version 3.0. Berkeley Geochronology Center, Special Publication, pp 1–40.

Lundstrom CC, Glazner AF (2016) Silicic magmatism and the volcanic-plutonic connection. Elements. 12:91–96. https://doi.org/10.2113/gselements.12.2.91

Maniar P, Piccoli P (1989) Tectonic disermination of granitoids. Geol Soc Am Bull. 101:635–643. https://doi.org/10.1130/0016-7606(1989)101%3c0635:TDOG%3e2.3.CO;2

Middlemost EAK (1994) Naming material in the magama/igneous rocks system. Earth Sci Rev. 37:215–224. https://doi.org/10.1016/0012-8252(94)90029-9

Miller CF (1985) Are strongly peraluminous magmas derived from politic sedimentary sources? J Geol. 93:673–689. https://doi.org/10.1086/628995

Pan G, Ding J, Yao D, Wang L (2004) Geological Map of Qinghai-Xiang (Tibet) Plateau and adjacent areas: Chengdu, China, Chengdu Institute of Geology and Mineral Resources, China Geological Survey. Chengdu Cartographic Publishing House, scale 1:1,500,000 (**in Chinese**).

Patiño Douce AE, Beard JS (1996) Effects of P, f(O_2) and Mg/Fe ratio on dehydration melting of model metagreywackes. J Petrol. 37:999–1024. https://doi.org/10.1093/petrology/37.5.999

Pearce JA, Harris NBW, Tindle AG (1984) Trace element discrimination diagrams for the tectonic interpretation of granitic rocks. J Petrol. 25:956–983. https://doi.org/10.1093/petrology/25.4.956

Peccerillo A, Taylor SR (1976) Geochemistry of Eocene calc-alkaline volcanic rocks from the Kastamonu area, Northern Turkey. Contrib Mineral Petrol. 58:63–81. https://doi.org/10.1007/BF00384745

Peng YB, Yu SY, Zhang JX, Li SZ, Tong LX, Sun DY (2017) Early Paleozoic arc magmatism and metamorphism in the northern Qilian Block, western China: Petrological and geochronological constraints. Geol J. 52:339–364. https://doi.org/10.1002/gj.3041

Rudnick RL, Gao S (2003) Composition of the continental crust. Treat Geochem. 3:1–64. https://doi.org/10.1016/B0-08-043751-6/03016-4

Rushmer T (1991) Partial melting of two amphibolites: Contrasting experimental results under fluid-absent conditions. Contrib Mineral Petrol. 107:41–59. https://doi.org/10.1007/BF00311184

Smith AD, Yang HY (2006) The neodymium isotopic and geochemical composition of serpentinites from ophiolitic assemblages in the Qilian foldbelt, northwest China. J Asian Earth Sci. 28:119–132. https://doi.org/10.1016/j.jseaes.2005.09.013

Smith AD (2006) The geochemistry and age of ophiolitic strata of the Xinglongshan Group: implications for the amalgamation of the Central Qilian belt. J Asian Earth Sci. 28(2–3):133–142. https://doi.org/10.1016/j.jseaes.2005.09.014

Song SG, Niu YL, Su L, Xia XH (2013) Tectonics of the north Qilian orogeny, NW China. Gondwana Res. 23:1378–1401. https://doi.org/10.1016/j.gr.2012.02.004

Song SG, Zhang LF, Niu YL, Wei CJ, Liou JG, Shu GM (2007) Eclogite and carpholite-bearing metasedimentary rocks in the North Qilian suture zone, NW China: Implications for Early Palaeozoic cold oceanic subduction and water transport into mantle. J Metamorp Geol. 25:547–563. https://doi.org/10.1016/j.jseaes.2008.11.005

Song SG, Zhang LF, Niu YL, Su L, Song B, Liu DY (2006) Evolution from oceanic subduction to continental collision: a case study from the Northern Tibetan Plateau based on geochemical and geochronological data. J Petrol. 47:435–455. https://doi.org/10.1093/petrology/egi080

Song SG, Niu Y, Zhang LF, Wei CJ, Liou JG, Su L (2009) Tectonic evolution of Early Paleozoic HP metamorphic rocks in the North Qilian Mountains, NW China: New perspectives. J Asian Earth Sci. 35:334–353. https://doi.org/10.1016/j.jseaes.2008.11.005

Song SG, Niu YL, Su L, Zhang C, Zhang LF (2014) Continental orogenesis from ocean subduction, continent collision/subduction, to orogen collapse, and orogen recycling: The example of the North Qaidam UHPM belt, NW China. Earth Sci Rev. 129:59–84. https://doi.org/10.1016/j.earscirev.2013.11.010

Sun SS, McDonough WF (1989) Chemical and isotopic systematics of oceanic basalts: Implications for mantle composition and processes. Geol Soc. 42:313–345. https://doi.org/10.1144/GSL.SP.1989.042.01.19

Sylvester PJ (1998) Post-collisional strongly peraluminous granites. Lithos. 45:29–44. https://doi.org/10.1016/S0024-4937(98)00024-3

Tang SH, Wang JH, Zhu XK, Ma HY (2007) Determination of strontium isotopic composition in celestite. Rock Mineral Anal. 26:93–96. (**in Chinese with English abstract**).

Taylor SR, Mclennan SM (1985) The continental crust: Its composition and evolution. J Geol. 94:57–72. https://doi.org/10.1086/629067

Tseng CY, Yang HJ, Yang HY, Liu D, Wu C, Cheng CK, Chen CH, Ker CM (2009) Continuity of the North Qilian and North Qinling orogenic belts, central orogenic system of China: Evidence from newly discovered Paleozoic adakitic rocks. Gondwana Res. 16:285–293. https://doi.org/10.1016/j.gr.2009.04.003

Wang N, Wu CL, Lei M, Chen HJ (2018) Petrogenesis and tectonic implications of the Early Paleozoic granites in the western segment of the North Qilian orogenic belt, China. Lithos. 312–313:89–107. https://doi.org/10.1016/j.lithos.2018.04.023

Wang TG, Li H, Liu JS, Evans NJ, Wang YC, Zha DH (2019) Whole-rock and zircon geochemistry of the Xiaoliugou granites, North Qilian Orogen (NW China): Implications for tectonic setting, magma evolution and W-Mo mineralization. Ore Geol Rev. 115:103166. https://doi.org/10.1016/joregeorev.2019.103166

Wang YC, Li H, Liu JS, Wang TG, Zha DH, Huang CW, Zhang CG (2020) Genesis of W-Mo mineralization in the Xiaoliugou and Ta'ergou ore fields, North Qilian Orogen (NW China): Constraints from fluid inclusions and S-Pb-H-O-Nd isotopes. Ore Geol Rev. 124:103649. https://doi.org/10.1016/j.oregeorev.2020.103649

Whalen JB, Currie KL, Chappell BW (1987) A-type granites: Geochemical characteristics, discrimination and petrogenesis. Contrib Mineral Petrol. 95:407–419. https://doi.org/10.1007/BF00402202

Wu CL, Xu XY, Gao QM, Li XM, Lei M, Gao YH, Frost R, Wooden JL (2010) Early Palaezoie granitoid magmatism and tectonic evolution in North Qilian, NW China. Acta Petrol Sin. 26:1027–1044. (**in Chinese with English abstract**).

Wu FY, Li XH, Yang JH, Zheng YF (2007) Discussions on the petrogenesis of granites. Acta Petrol Sin. 23:1217–1238 (**in Chinese with English abstract**).

Xia LQ, Li XM, Yu JY, Wang GQ (2016) Mid-late Neoproterozoic to Early Paleozoic volcanism and tectonic evolution of the Qilianshan, NW China. Geo Res J. 9–12:1–41. https://doi.org/10.1016/j.grj.2016.06.001

Xia LQ, Xia ZC, Zhao JT, Xu XY, Yang HQ, Zhao DH (1999) Determination of properties of Proterozoic continental flood basalts of western part from North Qilian Mountains. Sci China (Ser D Earth Sci). 42:506–514. https://doi.org/10.1007/BF02875244

Xia LQ, Xia ZC, Xu XY (2003) Magmagenesis in the Ordovician in back basins of the northern Qilian Mountains, China. Geol Soc Am Bull. 115:1510–1522. https://doi.org/10.1130/B25269.1

Xia XH, Song SG, Niu YL (2012) Tholeiite-boninite terrane in the North Qilian suture zone: Implications for subduction initiation and back-arc basin development. Chem Geol. 328:259–277. https://doi.org/10.1016/j.chemgeo.2011.12.001

Xiao WJ, Windley BF, Yong Y, Yan Z, Yuan C, Liu CZ, Li JL (2009) Early Paleozoic to Devonian multiple-accretionary model for the Qilian Shan, NW China. J Asian Earth Sci. 35:323–333. https://doi.org/10.1016/j.jseaes.2008.10.001

Xu YJ, Du YS, Cawood PA, Guo H, Huang H, An ZH (2010) Detrital zircon record of continental collision: Assembly of the Qilian Orogen, China. Sediment Geol. 230:35–45. https://doi.org/10.1016/j.sedgeo.2010.06.020

Yang H, Zhang HF, Luo BJ, Gao Z, Guo L, Xu WC (2016) Generation of peraluminous granitic magma in a post-collisional setting: A

case study from the eastern Qilian orogeny, NE Tibetan Plateau. Gondwana Res. 36:28–45. https://doi.org/10.1016/j.gr.2016.04.006

Yang XQ, Zhang ZH, Jiang ZS, Duan SG (2018) Geochronology, petrogenesis and tectonic significance of Huashugou granitoids in North Qilian, NW China. Lithos. 314–315:497–505. https://doi.org/10.1016/j.lithos.2018.06.023

Yin A, Harrison TM (2000) Geologic evolution of the Himalayan-Tibetan orogen. Annu Rev Earth Planet Sci. 28:211–280. https://doi.org/10.1146/annurev.earth.28.1.211

Yu S, Zhang J, Qin H, Sun D, Zhao X, Cong F, Li Y (2015) Petrogenesis of the Early Paleozoic low-Mg and high-Mg adakitic rocks in the North Qilian orogenic belt, NW China: Implications for transition from crustal thickening to extension thinning. J Asian Earth Sci. 107:122–139. https://doi.org/10.1016/j.jseaes.2015.04.018

Yuan W, Yang ZY (2015) Late Devonian closure of the North Qilian Ocean: Evidence from detrital zircon U-Pb geochronology and Hf isotopes in the eastern North Qilian Orogenic Belt. Int Geol Rev. 1(2):57. https://doi.org/10.1080/00206814.2014.999357

Zartman RE, Doe BR (1981) Plumbotectonics—the model. Tectonophysics. 75:135–162. https://doi.org/10.1016/0040-1951(81)90213-4

Zeng R, Lai J, Mao X, Li B, Ju P, Tao S (2016) Geochemistry, zircon U-Pb dating and Hf isotope composition of Paleozoic granitoids in Jinchuan, NW China: constraints on their petrogenesis, source characteristics and tectonic implication. J Asian Earth Sci. 121:20–33. https://doi.org/10.1016/j.jseaes.2016.02.009

Zindler A, Hart SR (1986) Chemical geodynamics. Annu Rev Earth Planet Sci. 14:493–571. https://doi.org/10.1146/annurev.ea.14.050186.002425

Zhang HF, Zhang BR, Harris N, Zhang L, Chen YL, Chen NS, Zhao ZD (2006) U-Pb zircon SHRIMP ages, geochemical and Sr-Nd-Pb isotopic compositions of intrusive rocks from the Longshan-Tianshui area in the southeast corner of the Qilian orogenic belt, China: Constraints on petrogenesis and tectonic affinity. J Asian Earth Sci. 27:751–764. https://doi.org/10.1016/j.jseaes.2005.07.008

Zhang JX, Xu ZQ, Chen W, Xu HF (1997) A tentative discussion on the ages of the subduction–accretionary complex/volcanic arcs in the middle sector of north Qilian Mountains. Acta Petrol Mineral. 16:112–119. (**in Chinese with English abstract**).

Zhang LQ, Zhang HF, Zhang SS, Xiong ZL, Luo BJ, Yang H, Pan FB, Zhou XC, Xu WC, Guo L (2017) Lithospheric delamination in post-collisional setting: Evidence from intrusive magmatism from the North Qilian orogen to southern margin of the Alxa block, NW China. Lithos. 288:20–34. https://doi.org/10.1016/j.lithos.2017.07.009

Zhang JX, Li JP, Yu SY, Meng FC, Mattinson CG, Yang HJ, Ker CM (2012) Provenance of eclogitic metasediments in the north Qilian HP/LT metamorphic terrane, western China: Geodynamic implications for Early Paleozoic subduction-erosion. Tectonophysics. 570–571:78–101. https://doi.org/10.1016/j.tecto.2012.08.018

Zhang JX, Meng FC, Wan YS (2007) A cold Early Paleozoic subduction zone in the north Qilian Mountains, NW China: Petrological and UPb geochronological constraints. J Metamorp Geol. 25:285–304. https://doi.org/10.1111/j.1525-1314.2006.00689.x

Zhao JL, Zhang X, Wang JR, Tang QY, Zhou WN, Ma XX (2022) Syn-orogenic tectonomagmatic evolution of the Qilian Orogen: Insights from the Lumanshan gabbro–granite association in the Qilian Block, Northwest China. Lithos. 434–435:106922. https://doi.org/10.1016/j.lithos.2022.106922

Zhao XM, Zhang ZH, Liu M, Li YS, Guo SF (2014) Zircon U-Pb geochronology, geochemistry and petrogenesis of the granites from the Xiaoliugou deposit in the western of the North Qilian. Acta Petrol Sin. 30:16–34 (**in Chinese with English abstract**).

Zhou ZM, Ma CQ, Wang LX, Chen SG, Xie CF, Li Y, Liu W (2017) A source-depleted Early Jurassic granitic pluton from South China: Implication to the Mesozoic juvenile accretion of the South China crust. Lithos. 300–301:278–290. https://doi.org/10.1016/j.lithos.2017.11.017

Zhu DC, Mo XX, Wang LQ, Zhao ZD, Niu YL, Zhou CY, Yang YH (2009) Petrogenesis of highly fractionated I-type granites in the Zayu area of eastern Gangdese, Tibet: Constraints from zircon U-Pb geochronology, geochemistry and Sr-Nd-Hf isotopes. Sci China (Ser D, Earth Sci). 52:1223–1239. https://doi.org/10.1007/s11430-009-0132-x

Zhu XH, Chen DL, Feng YM, Ren YF, Zhang X (2022) Granitic magmatism and tectonic evolution in the Qilian Mountain Range in NW China: A review. Earth Sci Front. 29:241–260 (**in Chinese with English abstract**).

Zuza AV, Wu C, Reith RC, Yin A, Li JH, Zhang JY, Zhang YX, Wu L, Liu WC (2017) Tectonic evolution of the Qilian Shan: An Early Paleozoic orogen reactivated in the Cenozoic. Geol Soc Am Bull. 130:881–925. https://doi.org/10.1130/b31721.1